

The Higgs and Leptophobic Force at the LHC

Pavel Fileviez Pérez,^a Elliot Golias,^a Clara Murgui^b and Alexis D. Plascencia^a

^a*Physics Department and Center for Education and Research in Cosmology and Astrophysics (CERCA), Case Western Reserve University, Cleveland, OH 44106, USA*

^b*Departamento de Física Teórica, IFIC, Universitat de Valencia-CSIC, E-46100, Valencia, Spain*

E-mail: pxf112@case.edu, ebg23@case.edu, clara.murgui@ific.uv.es,
alexis.plascencia@case.edu

ABSTRACT: The Higgs boson could provide the key to discover new physics at the Large Hadron Collider. We investigate novel decays of the Standard Model (SM) Higgs boson into leptophobic gauge bosons which can be light in agreement with all experimental constraints. We study the associated production of the SM Higgs and the leptophobic gauge boson that could be crucial to test the existence of a leptophobic force. Our results demonstrate that it is possible to have a simple gauge extension of the SM at the low scale, without assuming very small couplings and in agreement with all the experimental bounds that can be probed at the LHC.

1 Introduction

The discovery of the Standard Model (SM) Higgs boson with a mass of 125 GeV at the Large Hadron Collider (LHC) [1, 2] can be considered one of the most important discoveries in physics. We now understand how most of the elementary particles acquire mass through the Higgs mechanism and how the electroweak symmetry is spontaneously broken in nature. Thanks to the great effort of the experimental collaborations at the LHC we know well the properties of the SM Higgs and there exist experimental constraints on its decays and production mechanisms, see for example Ref. [3] for a detailed discussion.

The Higgs boson could open a door to a new physics sector since it can have new interactions that can provide information about a theory for physics beyond the Standard Model. The LHC could discover new decays and/or production channels for the Higgs boson and combining different searches we could have access to new interactions and discover new particles with masses below the TeV scale. See Ref. [4] for a report on future studies at the LHC.

In this article, we investigate new possible decays and production mechanisms of the Higgs boson due to the existence of a new interaction with a leptophobic gauge boson. A leptophobic gauge boson is predicted in simple theories where baryon number is a local gauge symmetry [5–8] spontaneously broken at the low scale. See Refs. [9–11] for realistic models predicting a leptophobic gauge boson and Ref. [12] for a review. In our studies we show that one can have a large branching ratio for the Higgs decays into two leptophobic gauge bosons if they are kinematically allowed. The leptophobic gauge boson can be light with mass below the electroweak scale in agreement with all experimental bounds and without assuming a very small gauge coupling.

When the new Higgs decays are highly suppressed or not allowed we investigate the associated Higgs-leptophobic gauge boson production mechanism at the LHC. We find that, using this production mechanism, one can obtain large number of events with multi-photons and two quarks that can be used to test the existence of a new interaction of the Higgs boson with this new gauge boson. As in the case of the Higgs decays, the production cross-sections can be generically large due to the fact that the leptophobic gauge boson can be light in agreement with all experimental bounds. The possible existence of a leptophobic gauge boson at the low scale tells us that a gauge theory where baryon number is a local symmetry [8–11] can describe physics below the TeV scale.

This article is organized as follows: In Section 2, we review all current collider constraints on a leptophobic gauge boson and discuss the impact of these bounds on the predictions for production cross-sections at the LHC. In Section 3, we show the predictions for the new Higgs decay channels into two leptophobic gauge bosons taking into account all the experimental constraints. In Section 4, we discuss the associated production channel proton-proton to the leptophobic gauge boson and the SM Higgs, $pp \rightarrow Z_B^* \rightarrow Z_B h$, and investigate the different signatures at the LHC. We present our conclusions in Section 5. Appendices A and B contain analytic results for all the processes considered in this work. In Appendix C, we discuss the bounds on the kinetic mixing between the Z and the new gauge boson.

2 Leptophobic Gauge Boson at the LHC

In simple extensions of the SM where baryon number is a local symmetry [8–11] spontaneously broken one predicts the existence of a leptophobic gauge boson Z_B . For phenomenological studies of these models and dark matter see Refs. [13–17], while for a mechanism for baryogenesis in this scenario see Ref. [18]. The coupling between the SM quarks and Z_B in our convention is given by

$$Z_B^\mu \bar{q}q : -i\frac{g_B}{3}\gamma^\mu. \quad (2.1)$$

As we show in the following, the local baryon number can be broken at the low scale, even at energies below the electroweak scale.

The main strategy to search for a heavy Z_B at the LHC is by looking for a dijet resonance. However, at low masses this search loses sensitivity due to the large QCD backgrounds. Nonetheless, recent experimental searches for a boosted leptophobic gauge boson decaying into jets along with initial state radiation of a photon have been performed at CMS to place exclusion bounds down to a mass of 10 GeV for Z_B [19]. This further motivates a study in the low mass region.

In Fig. 1 we summarize the current collider bounds for the leptophobic gauge boson in the $g_B - M_{Z_B}$ plane. As this figure shows, there is a large region in the parameter space that remains unconstrained. Specifically, for a light Z_B with mass between 25 and 50 GeV the gauge coupling can take relatively large values. For smaller couplings, i.e. $g_B \lesssim 0.1$, almost any value in the window $25 \text{ GeV} < M_{Z_B} < 1 \text{ TeV}$ is allowed. Therefore, there is hope to produce this gauge boson at the LHC with large cross-sections and study its properties.

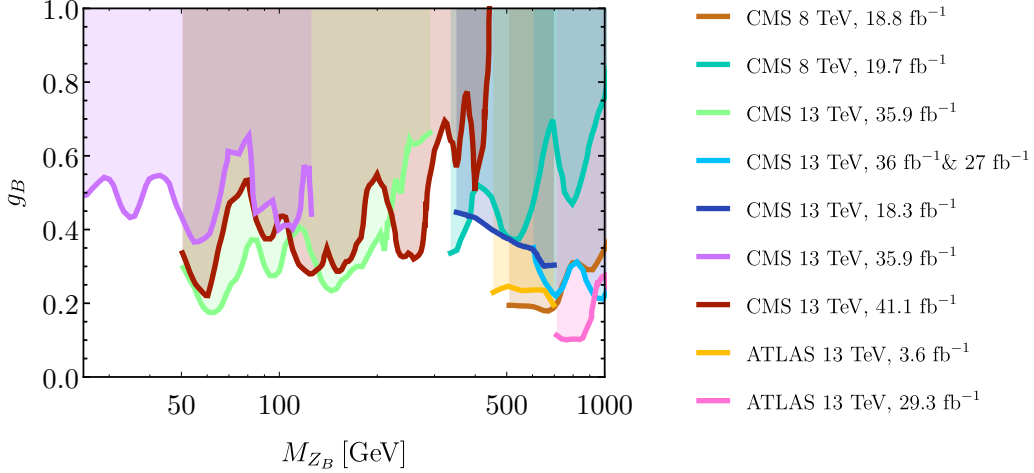


Figure 1: Experimental bounds for the leptophobic gauge boson Z_B . Here, we use the CMS analyses (8 TeV and 18.8 fb^{-1} [20], 8 TeV and 19.7 fb^{-1} [21], 13 TeV and 35.9 fb^{-1} [19, 22] and 41.1 fb^{-1} [22], 13 TeV and 36 fb^{-1} & 27 fb^{-1} [23], 13 TeV and 18.3 fb^{-1} [24]), and ATLAS results (13 TeV and 3.6 fb^{-1} and 29.3 fb^{-1} [25]).

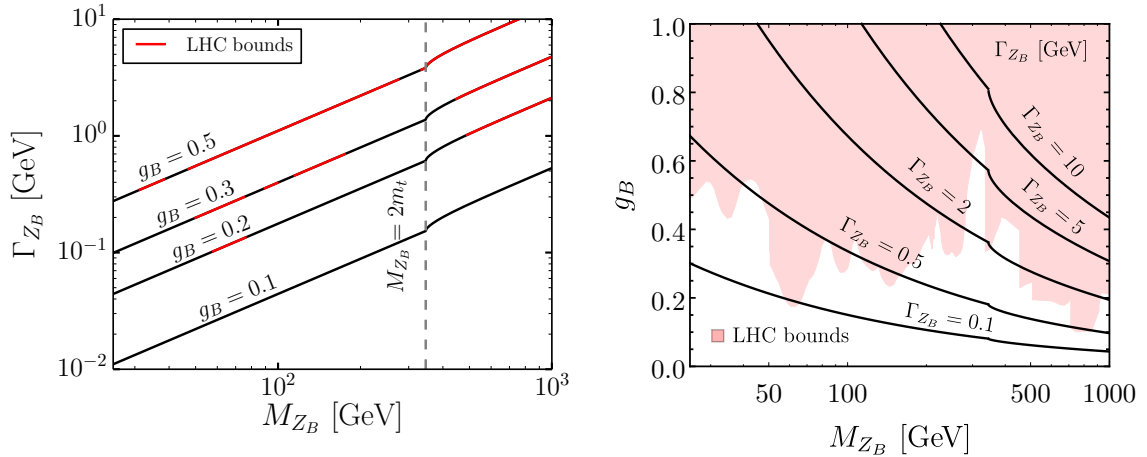


Figure 2: *Left panel:* Decay width of the Z_B boson as a function of its mass. The regions highlighted in red are excluded by searches at the LHC. To the right of the dashed vertical line the decay channel $Z_B \rightarrow t\bar{t}$ is open. *Right panel:* Contour lines for the decay width of the Z_B boson in the g_B vs M_{Z_B} plane.

In the left panel in Fig. 2 we show the decay width of Z_B for different values of the gauge coupling g_B as a function of its mass. In red we show the regions that are ruled out by the collider bounds shown in Fig. 1. From this we can infer which are the allowed values for the decay width of the leptophobic gauge boson. Moreover, with this information of the decay width we can predict the different cross-sections relevant for different collider searches. In the right panel in Fig. 2 we present contours of Γ_{Z_B} in the g_B vs M_{Z_B} plane. The region shaded in red is excluded by collider searches of the Z_B and we conclude that a Γ_{Z_B} of order GeV is already mostly excluded.

In Fig. 3 we present our results for the production cross-section for different channels that involve at least one Z_B , fixing the gauge coupling to $g_B = 0.2$. These results correspond to the LHC with center-of-mass energy of 14 TeV and the number of events shown on the right vertical axis corresponds to an integrated luminosity of 300 fb^{-1} . The model has been implemented in `FeynRules 2.0` [26] and the cross-sections obtained using `MadGraph5aMC@NLO - v2.7.0` [27], we cross-checked our results in a `Mathematica` notebook and the use of the MSTW2008 [28] set of parton distribution functions. In Appendices A and B we provide analytic results for all the processes we have considered.

From Fig. 3 one can see that the dijet cross-section dominates across the plot, and in the region $M_{Z_B} > 2M_t$ the process $pp \rightarrow Z_B \rightarrow t\bar{t}$ can be large as well. The process $pp \rightarrow Z_B q$ can be significant, since there is a large contribution from the parton distribution function of the gluon in the initial state. For the $pp \rightarrow Z_B \gamma$, $Z_B q$ and $Z_B g$ channels we impose the following cuts on the rapidity and the transverse momentum: $|\eta| < 2.5$, and $p_T > 150 \text{ GeV}$. These three channels are relevant for searches in the low mass regime.

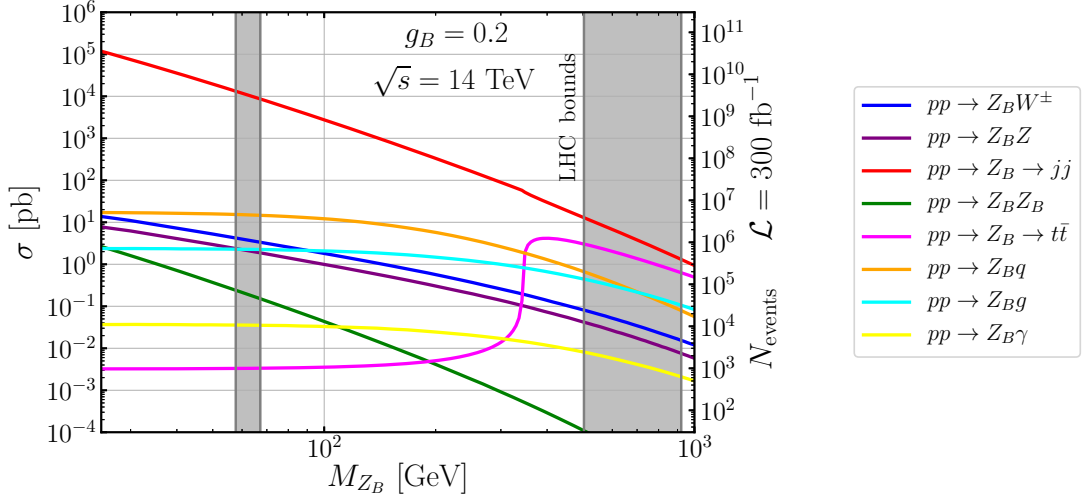


Figure 3: Production cross-sections at the LHC for center-of-mass energy of 14 TeV in units of picobarns, we fixed $g_B = 0.2$. On the right side of the vertical axis we show the expected number of events assuming 300 fb^{-1} for the integrated luminosity. The regions shaded in gray are excluded by LHC searches for the Z_B boson.

3 Exotic Decays of the SM-like Higgs

In extensions of the SM with a leptophobic gauge boson [8–11], its mass generation comes from the vacuum expectation of a new Higgs boson with non-zero baryon number, and hence, the models have two Higgs scalars that can mix with each other. After spontaneous

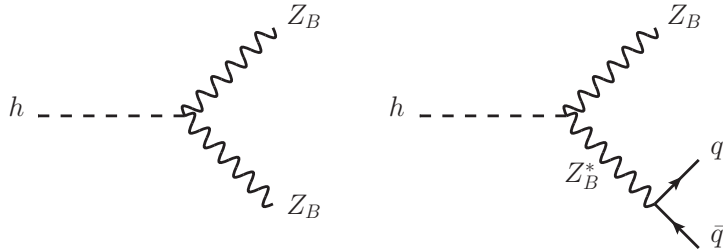


Figure 4: Higgs decays into leptophobic gauge bosons.

symmetry breaking, the SM-like Higgs will have the following coupling to the leptophobic Z_B gauge boson

$$h Z_B^\mu Z_B^\nu : 2i \frac{M_{Z_B}^2}{v_B} g^{\mu\nu} \sin \theta_B, \quad (3.1)$$

where θ_B is the mixing angle in the scalar sector, $M_{Z_B} = Q_B g_B v_B$ and Q_B is the baryon number of the second scalar. Since the leptophobic gauge boson can be light, the SM-like Higgs can have the following decays

$$h \rightarrow Z_B Z_B, Z_B^* Z_B,$$

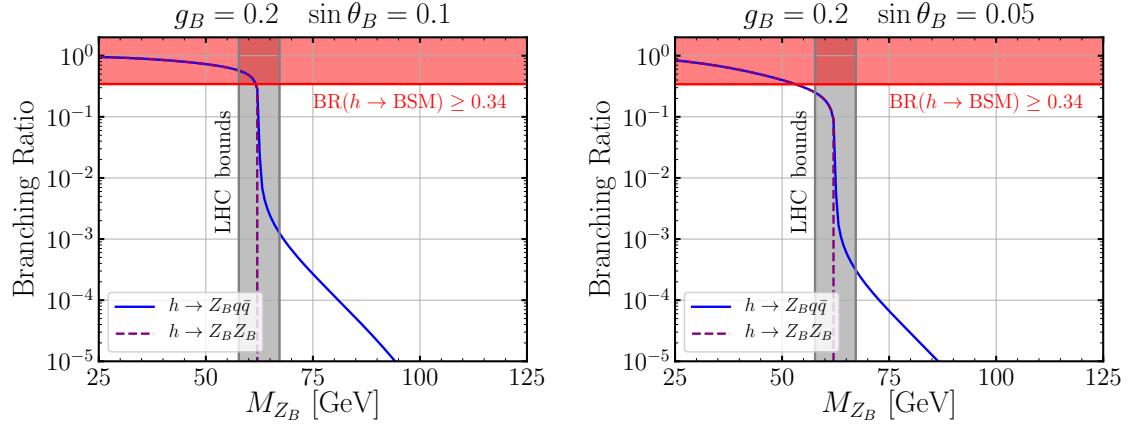


Figure 5: Branching ratios for the channels $h \rightarrow Z_B Z_B$ and $h \rightarrow Z_B Z_B^* \rightarrow Z_B q\bar{q}$. The left (right) panel corresponds to $g_B = 0.2$ and $\sin \theta_B = 0.1$ ($\sin \theta_B = 0.05$). The region shaded in red shows the exclusion bounds from the constraint on the SM-like Higgs branching ratio $\text{BR}(h \rightarrow \text{BSM}) < 0.34$. The region shaded in gray corresponds to the exclusion bounds from direct searches for the Z_B boson at the LHC.

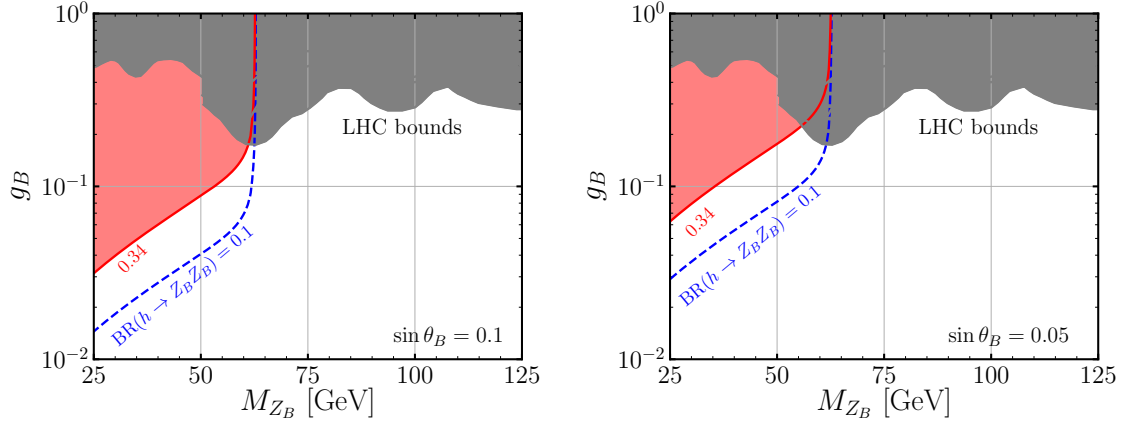


Figure 6: Exclusion bounds in the g_B vs M_{Z_B} plane. The region shaded in red shows the exclusion bounds from the constraint on the SM-like Higgs branching ratio $\text{BR}(h \rightarrow Z_B Z_B) < 0.34$, while the blue dashed line corresponds to $\text{BR}(h \rightarrow Z_B Z_B) = 0.1$. The region shaded in gray is excluded by searches for the Z_B at the LHC. The left (right) panel corresponds to $\sin \theta_B = 0.1$ ($\sin \theta_B = 0.05$).

depending on the Z_B mass, see Fig. 4. In order to calculate these decays one needs to know the coupling between the SM quarks and the Z_B . Notice that the couplings between the SM-like Higgs and SM particles will scale by a factor $\cos \theta_B$. With this information we can calculate the impact of these novel decays of the SM-like Higgs by computing the total Higgs decay width $\Gamma_h = \cos^2 \theta_B \Gamma_{\text{SM}} + \Gamma_{\text{BSM}}$, where in our case Γ_{BSM} corresponds to the decays into two leptophobic gauge bosons.

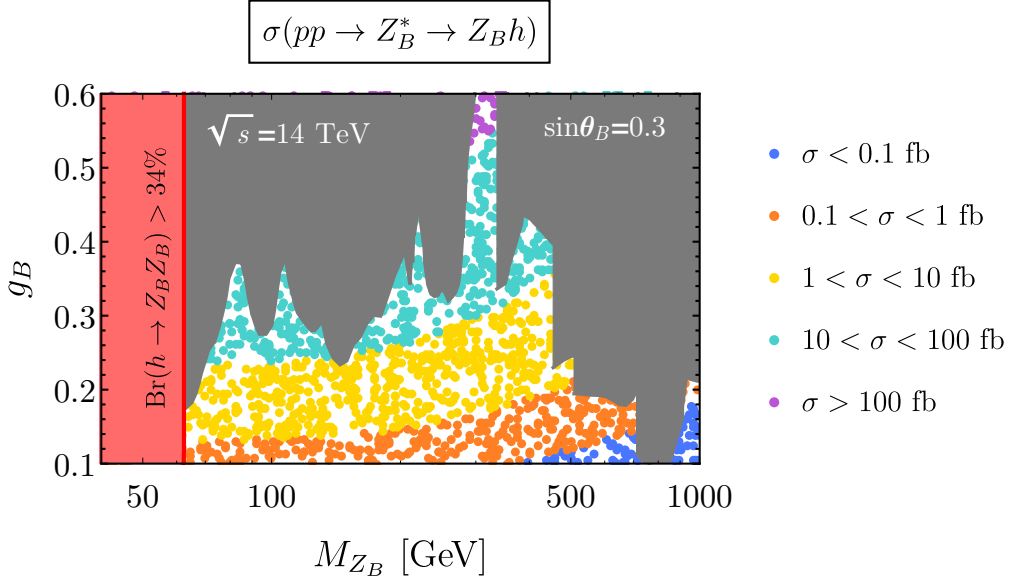


Figure 7: Predictions for the associated production cross-section $p p \rightarrow Z_B^* \rightarrow Z_B h$ at the LHC with center-of-mass energy of 14 TeV. The gray region is excluded by the LHC bounds, while the red region is excluded by the bound on the branching ratio of the new Higgs decays. The scalar mixing angle is fixed to $\sin \theta_B = 0.3$ for this plot.

Collider searches of a new scalar mixing with the SM Higgs combined with measurements of the SM Higgs properties provide constraints on the mixing angle. In our study we take the bound $\sin \theta_B \leq 0.3$ [29]. Current LHC measurements of the properties of the SM-like Higgs boson give the following constraint on its branching ratio into BSM particles [30]

$$\text{BR}(h \rightarrow \text{BSM}) < 0.34 \quad \text{at 95\% CL}, \quad (3.2)$$

which is obtained assuming the production of the Higgs in the SM. Therefore, we scale the bound by the ratio between the production cross-section for the Higgs in the SM with the one in this model, which is given by $\text{BR}(h \rightarrow \text{BSM}) < 0.34 \times (\sigma_h^{\text{SM}}/\sigma_h) = 0.34/\cos^2 \theta_B$.

We have computed the two-body and three-body decays and provide analytic expressions in Appendix A. In Fig. 5 we present our results for the branching ratios for the decay channels $h \rightarrow Z_B Z_B$ and $h \rightarrow Z_B q \bar{q}$ of the SM Higgs. The latter includes both, the on-shell and the off-shell contribution from the Z_B . In the region with $M_{Z_B} \leq M_h/2 \approx 62.5$ GeV the channel $h \rightarrow Z_B Z_B$ becomes the dominant decay channel and the Higgs decay width can become of order GeV. In this region the bound on $\text{BR}(h \rightarrow \text{BSM}) < 0.34$ gives a strong constraint shown by the area shaded in red. The gray band in this figure corresponds to the exclusion bounds from direct searches for the Z_B boson at the LHC discussed in Section 2.

On the other hand, when $M_{Z_B} \geq M_h/2$ the two-body decay is kinematically closed and the three-body decay gives a much smaller contribution to the Higgs width. In this regime, experiments can search for the associated Higgs Z_B production to probe the existence of these interactions, as we discuss in the following section.

The experimental bound on the branching ratio of Higgs decays to BSM particles can be translated to the g_B vs M_{Z_B} plane. Nevertheless, we note that this bound also depends on the scalar mixing. In Fig. 6 we present our results for two different mixing angles. For $\sin \theta_B = 0.1$ this constraint is strong in the region $M_{Z_B} \leq M_h/2$ and excludes $g_B \gtrsim 0.03$ for $M_{Z_B} = 25$ GeV. In order to relax this bound one needs to go to very small mixing angles, $\sin \theta_B < 0.05$, as shown in the right panel. It is important to emphasize that the SM-like Higgs can have a large branching ratio into two leptophobic gauge bosons in agreement with all current experimental bounds.

4 Higgs-Leptophobic Gauge Boson Associated Production

In the previous section we discussed the possible new Higgs decays due to the existence of a leptophobic gauge boson. In the scenarios where these Higgs decays are not allowed or highly suppressed, one can study the associated production

$$p p \rightarrow Z_B^* \rightarrow Z_B h,$$

to test the existence of the new $h - Z_B - Z_B$ interaction. See Fig. 8 for the relevant Feynman graph.

The production cross-section for this process is given by Eq. (B.4). In Fig. 7 we show the numerical predictions for the associated production $p p \rightarrow Z_B^* \rightarrow Z_B h$ in the $g_B - M_{Z_B}$ plane, in the maximal mixing scenario where $\sin \theta_B = 0.3$ and with center-of-mass energy of $\sqrt{s} = 14$ TeV. The region shaded in red is excluded by the experimental bound on the branching ratio of the SM Higgs into BSM particles discussed in the previous section. The different colored dotted regions correspond to the predictions in different ranges: $\sigma < 0.1$ fb (blue dots), $0.1 \text{ fb} < \sigma < 1$ fb (orange dots), $1 \text{ fb} < \sigma < 10$ fb (yellow dots), $10 \text{ fb} < \sigma < 100$ fb (cyan dots), and $\sigma > 100$ fb (purple dots). The production cross-section can easily be in the tens of femtobarns which is not too far from the $pp \rightarrow Zh$ cross-section of 990.33 fb in the SM [31]. The region shaded in gray is excluded by the collider bounds discussed in Section 2. The associated cross-section is proportional to $\sin^2 \theta_B$. Therefore, although in the above figure we show only the predictions for $\sin \theta_B = 0.3$, one can easily find the predictions values for other mixing angles. It is important to mention that the associated production can be significant due to the fact that the gauge coupling can be large and the mass of the leptophobic gauge boson can be below the electroweak scale.

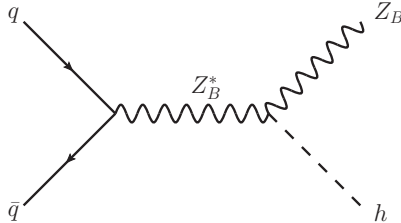


Figure 8: Associated $Z_B - h$ production channel.

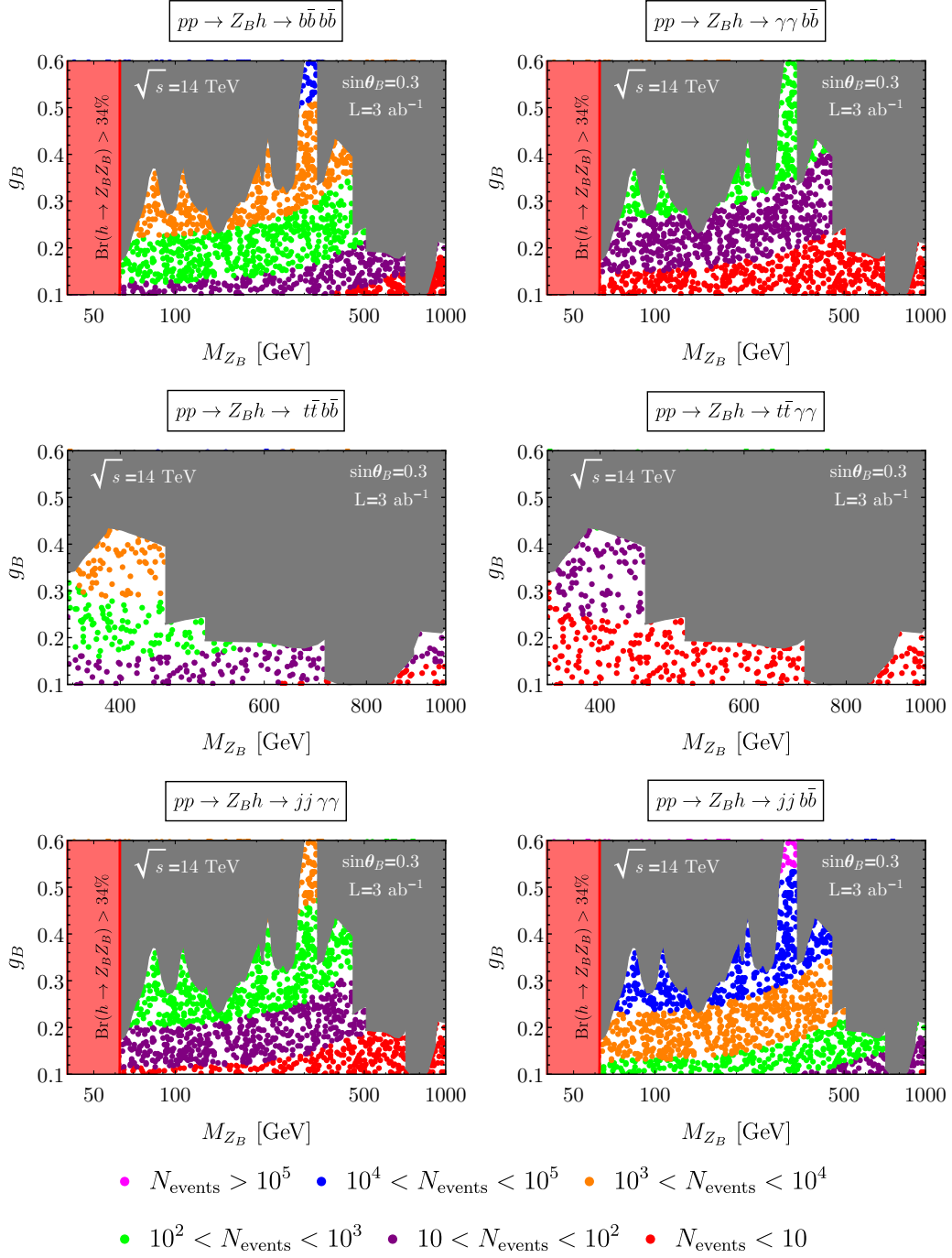


Figure 9: Predictions for the number of events at the LHC with center-of-mass energy of 14 TeV assuming that the integrated luminosity is $\mathcal{L} = 3000 \text{ fb}^{-1}$ and using the maximal allowed value for the mixing angle $\sin\theta_B = 0.3$. We show the number of events for the most relevant channels: $\gamma\gamma t\bar{t}$, $\gamma\gamma b\bar{b}$, $\gamma\gamma j j$, $b\bar{b}b\bar{b}$, $b\bar{b}t\bar{t}$, and $b\bar{b}j j$. The gray region is excluded by the LHC bounds, while the red region is excluded by the bound on the branching ratio of the new Higgs decays.

Knowing the possible h and Z_B decays we can show the predictions for the number of events at the LHC for the following channels:

$$\gamma\gamma\, t\bar{t}, \gamma\gamma\, b\bar{b}, \gamma\gamma\, jj, b\bar{b}b\bar{b}, b\bar{b}t\bar{t}, \text{ and } b\bar{b}jj.$$

The number of events for each of these channels is given by

$$N_{\text{events}}(x\bar{x}y\bar{y}) = \mathcal{L} \times \sigma(p\,p \rightarrow Z_B^* \rightarrow Z_B\,h) \times \text{BR}(h \rightarrow x\bar{x}) \times \text{BR}(Z_B \rightarrow y\bar{y}). \quad (4.1)$$

In Fig. 9 we show the predictions for the expected number of events assuming that the integrated luminosity is $\mathcal{L} = 3000\text{ fb}^{-1}$ as planned for the High-Luminosity LHC [32], and using the maximal allowed value for the mixing angle $\sin\theta_B = 0.3$. The gray regions in Fig. 9 are excluded by the collider bounds discussed in Section 2, while the regions in red are excluded by the experimental bound on the branching ratio of SM Higgs exotic decays.

The Zh associated production has been measured at ATLAS [33] and CMS [34], and a similar technique can be used to make the reconstruction of the processes in Fig. 9. However, in our case the Z_B decays only to quarks and then the QCD background is more challenging. For example, the largest number of events is for the channel: $pp \rightarrow Z_B h \rightarrow jjb\bar{b}$. In this case two b jets should have an invariant mass around the Higgs mass of 125 GeV. Furthermore, the large p_T of the Higgs or the gauge boson can help discriminate the signal with respect to the background [35]. A dedicated analysis for these signatures is required but it is beyond the scope of this article.

5 Summary

The SM Higgs boson can open a doorway to new physics and there is a chance to discover a new sector from the existence of new interactions with the Higgs. In this article, we investigated the possibility that the Higgs can have a new interaction with a leptophobic gauge boson. In this scenario, Higgs decays can have a large branching ratio into two leptophobic gauge bosons if they are kinematically allowed. The leptophobic gauge boson can be very light, with mass below the electroweak scale, in agreement with all experimental bounds and without assuming a very small gauge coupling.

In the case where the new Higgs decays are highly suppressed or not allowed, we investigated the associated production of the Higgs and the leptophobic gauge boson at the LHC. We showed that this channel can lead to a large number of events with multi-photons and two quarks, which can be used to probe the existence of the interaction of the Higgs with the new gauge boson. As in the case of the exotic Higgs decays, the production cross-sections can be generically large due to the fact that the leptophobic gauge boson can be light in agreement with all experimental bounds. It is relevant to mention that the possible existence of a leptophobic gauge boson at the low scale tells us that it is possible to have a simple gauge theory where baryon number is a local gauge symmetry [8–11] describing physics below the TeV scale.

Acknowledgments: The work of P.F.P. has been supported by the U.S. Department of Energy, Office of Science, Office of High Energy Physics, under Award Number DE-SC0020443. The work

of C.M. has been supported in part by Grants No. FPA2014-53631-C2-1-P, No. FPA2017-84445-P, and No. SEV-2014- 0398 (AEI/ERDF, EU), and by La Caixa-Severo Ochoa scholarship.

A Decays Widths

- Leptophobic Gauge Boson:

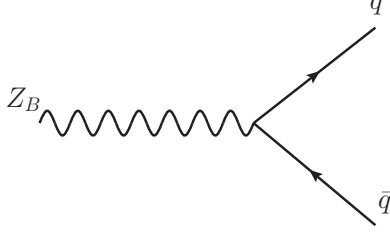


Figure 10: Leptophobic gauge boson decay.

The partial decay width of the leptophobic gauge boson Z_B with mass M_{Z_B} is given by

$$\Gamma(Z_B \rightarrow \bar{q}q) = \frac{g_B^2 M_{Z_B}}{36\pi} \sqrt{1 - \frac{4M_q^2}{M_{Z_B}^2}} \left(1 + \frac{2M_q^2}{M_{Z_B}^2} \right), \quad (\text{A.1})$$

where M_q is the mass of a given quark.

- New Higgs Decays:

The width for the new two-body decays, $h \rightarrow Z_B Z_B$, of the SM Higgs boson is

$$\Gamma(h \rightarrow Z_B Z_B) = \frac{G_B M_h^3 \sin^2 \theta_B}{16\sqrt{2}\pi} \sqrt{1 - 4x} (1 - 4x + 12x^2), \quad (\text{A.2})$$

with $x = M_{Z_B}^2/M_h^2$ and $G_B = 1/(\sqrt{2}v_B^2)$.

The three-body decay, $h \rightarrow Z_B(p_1) q(p_2) \bar{q}(p_3)$, is given by

$$\Gamma(h \rightarrow Z_B q \bar{q}) = \frac{1}{(2\pi)^3} \frac{1}{32M_h^3} \int_{p_{12}^{\min}}^{p_{12}^{\max}} dp_{12} \int_{p_{23}^{\min}}^{p_{23}^{\max}} dp_{23} |\bar{A}(h \rightarrow \bar{q}q Z_B)|^2. \quad (\text{A.3})$$

Neglecting the quark masses we have that

$$p_{12}^{\min} = M_{Z_B}^2, \quad p_{12}^{\max} = M_h^2, \quad (\text{A.4})$$

$$p_{23}^{\min} = 0, \quad p_{23}^{\max} = \frac{1}{p_{12}} (p_{12} - M_{Z_B}^2)(M_h^2 - p_{12}), \quad (\text{A.5})$$

where $p_{ij} = (p_i + p_j)^2$ and the spin-averaged squared amplitude is given by

$$\begin{aligned} |\bar{A}(h \rightarrow \bar{q}q Z_B)|^2 &= \frac{8 g_B^2}{3 v_B^2} \frac{M_{Z_B}^4 \sin^2 \theta_B}{\left((p_{23} - M_{Z_B}^2)^2 + M_{Z_B}^2 \Gamma_{Z_B}^2 \right)} \\ &\times \left(p_{23} + \frac{(p_{12} - M_{Z_B}^2)(M_h^2 - p_{12} - p_{23})}{M_{Z_B}^2} \right). \end{aligned} \quad (\text{A.6})$$

B Production Cross-sections

The hadronic production cross-section reads as

$$\sigma(pp \rightarrow XY)(s) = \int_{\tau_0}^1 d\tau \frac{d\mathcal{L}_{q\bar{q}}^{pp}}{d\tau} \sigma(q\bar{q} \rightarrow XY)(\hat{s}), \quad (\text{B.1})$$

where $\sigma(q\bar{q} \rightarrow XY)(\hat{s})$ corresponds to the partonic cross-section and

$$\frac{d\mathcal{L}_{q\bar{q}}^{pp}}{d\tau} = \int_{\tau}^1 \frac{dx}{x} \left[f_{q/p}(x, \mu) f_{\bar{q}/p}\left(\frac{\tau}{x}, \mu\right) + f_{q/p}\left(\frac{\tau}{x}, \mu\right) f_{\bar{q}/p}(x, \mu) \right]. \quad (\text{B.2})$$

The parameter $\tau = \hat{s}/s$, where \hat{s} is the partonic center-of-mass energy squared, s is the hadronic center-of-mass energy squared, $\tau_0 = (M_X + M_Y)^2/s$ is the production threshold, and μ is the factorization scale. In what follows we give the analytic results for the partonic cross-sections.

- Di-quark production:

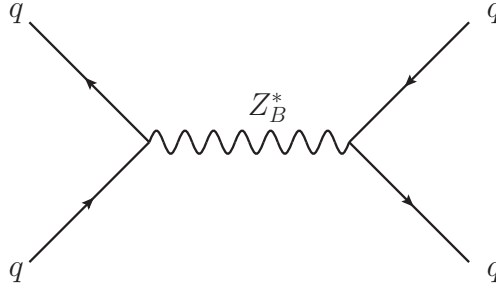


Figure 11: Di-quark production channel.

The di-quark production cross-section through the leptophobic gauge boson,

$$\bar{q}q \rightarrow Z_B^* \rightarrow \bar{q}q,$$

is given by

$$\sigma(\bar{q}q \rightarrow Z_B^* \rightarrow \bar{q}q)(\hat{s}) = \frac{g_B^4 \sqrt{\hat{s} - 4M_q^2}}{972\pi\sqrt{\hat{s}}} \frac{(2M_q^2 + \hat{s})}{\left[(\hat{s} - M_{Z_B}^2)^2 + M_{Z_B}^2 \Gamma_{Z_B}^2\right]}, \quad (\text{B.3})$$

where we have neglected the quark masses in the initial state.

- Associated Production:

The associated $Z_B - h$ production,

$$pp \rightarrow Z_B^* \rightarrow Z_B h,$$

is relevant to test the existence of the new Higgs interaction with the leptophobic gauge boson.

The cross-section at the partonic level is given by

$$\sigma(\bar{q}q \rightarrow Z_B^* \rightarrow Z_B h)(\hat{s}) = \frac{g_B^4 \sin^2 \theta_B}{144\pi \hat{s}^2} \frac{\left[\hat{s}^2 - 2\hat{s}(M_{Z_B}^2 + M_h^2) + (M_{Z_B}^2 - M_h^2)^2 \right]^{1/2}}{\left[(\hat{s} - M_{Z_B}^2)^2 + M_{Z_B}^2 \Gamma_{Z_B}^2 \right]} \times \left[\hat{s}^2 + 2\hat{s}(5M_{Z_B}^2 - M_h^2) + (M_{Z_B}^2 - M_h^2)^2 \right], \quad (\text{B.4})$$

where the $U(1)_B$ charge of the new scalar is taken as $Q_B = 3$ as in the minimal models [8–11].

- Di-boson production:

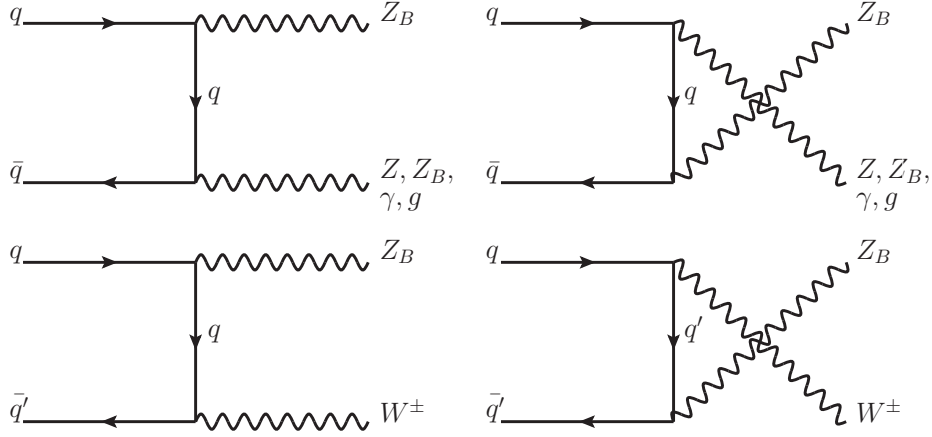


Figure 12: Di-boson production channels.

Taking the quarks to be massless, the cross-section for the process $q\bar{q} \rightarrow Z_B V$ where $V = Z, W^\pm, Z_B$ is given by

$$\sigma(q\bar{q} \rightarrow Z_B V)(s) = \frac{n g_B^2 (C_V^2 + C_A^2)}{108\pi s^2} \left[-2\sqrt{f(s)} + \frac{(M_V^2 + M_{Z_B}^2)^2 + s^2}{s - M_V^2 - M_{Z_B}^2} \log \left(\frac{\sqrt{f(s)} + s - M_V^2 - M_{Z_B}^2}{\sqrt{f(s)} - s + M_V^2 + M_{Z_B}^2} \right) \right] \quad (\text{B.5})$$

where the overall factor $n = 1 (= 1/2)$ corresponds to having distinguishable (indistinguishable) particles in the final state,

$$f(s) \equiv M_V^4 - 2M_V^2(M_{Z_B}^2 + s) + (M_{Z_B}^2 - s)^2, \quad (\text{B.6})$$

and the coefficients C_V and C_A correspond to the vector and axial couplings of the

gauge bosons respectively,

$$Z_B Z : C_V = \frac{g_2}{\cos \theta_W} \left(\frac{1}{2} T_q^3 - Q_q \sin^2 \theta_W \right), \quad C_A = -\frac{g_2}{2 \cos \theta_W} T_q^3 \quad (\text{B.7})$$

$$Z_B W^\pm : C_V = \frac{g_2}{2\sqrt{2}}, \quad C_A = -\frac{g_2}{2\sqrt{2}} \quad (\text{B.8})$$

$$Z_B Z_B : C_V = \frac{g_B}{3}, \quad C_A = 0. \quad (\text{B.9})$$

- For the process $q\bar{q} \rightarrow Z_B \gamma$ the averaged squared amplitude is given by,

$$|\overline{\mathcal{M}}(q\bar{q} \rightarrow Z_B \gamma)|^2 = \frac{2 e^2 Q_q^2 g_B^2 [M_{Z_B}^4 - 2M_{Z_B}^2 t + s^2 + 2t(s+t)]}{27 t (M_{Z_B}^2 - s - t)}, \quad (\text{B.10})$$

where Q_q corresponds to the electric charge of the quark. In order to compute the proton-proton cross-section we include the cuts on the transverse momentum and the rapidity of the photon (also gluon and quark) as it is explained in the main text.

- For the process $q\bar{q} \rightarrow Z_B g$ we have

$$|\overline{\mathcal{M}}(q\bar{q} \rightarrow Z_B g)|^2 = \frac{8 g_S^2 g_B^2 [M_{Z_B}^4 - 2M_{Z_B}^2 t + s^2 + 2t(s+t)]}{81 t (M_{Z_B}^2 - s - t)}, \quad (\text{B.11})$$

where g_S corresponds to the strong coupling the SM.

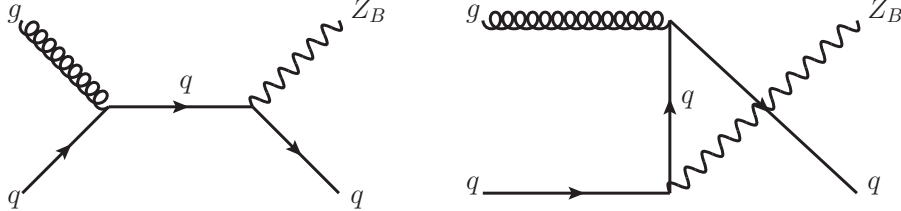


Figure 13: Feynman graphs for $gq \rightarrow Z_B q$.

- For the process $qg \rightarrow Z_B q$, the averaged squared amplitude is given by

$$|\overline{\mathcal{M}}(qg \rightarrow Z_B q)|^2 = \frac{g_B^2 g_S^2}{27} \frac{M_{Z_B}^4 - 2M_{Z_B}^2 s + 2s^2 + 2st + t^2}{s(s+t - M_{Z_B}^2)}, \quad (\text{B.12})$$

and we follow the same procedure as above to compute the proton-proton cross-section.

C Constraints from Kinetic Mixing

In this Appendix, we study the kinetic mixing between the $U(1)_Y$ and $U(1)_B$ gauge bosons, see Refs. [8–11] for realistic theories where baryon number is a local gauge symmetry. This parameter can be constrained by studying the properties of the Z boson in the SM, see e.g. [36, 37]. The most general Lagrangian that can be written under the gauge group $SU(3)_c \otimes SU(2)_L \otimes U(1)_Y \otimes U(1)_B$ involving the neutral gauge bosons of the theory is given by

$$\begin{aligned} \mathcal{L} \supset & -\frac{1}{4}B_{\mu\nu}B^{\mu\nu} - \frac{1}{2}\text{Tr } W_{\mu\nu}W^{\mu\nu} - \frac{1}{4}B'_{\mu\nu}B'^{\mu\nu} - \frac{\sin\epsilon}{2}B_{\mu\nu}B'^{\mu\nu} \\ & + \frac{1}{8}(g_2W_{3\mu} - g_1B_\mu)(g_2W_3^\mu - g_1B^\mu)v_0^2 + \frac{1}{2}\mu_{B'}^2B'_\mu B'^\mu \\ & - \sum_i \bar{\psi}_i \gamma^\mu [g_1(Y_L^i P_L + Y_R^i P_R)B_\mu + g_2 P_L T^a W_{a\mu}] \psi_i + g_B \sum_i \bar{\psi}_i \gamma^\mu Q_B \psi_i B'_\mu, \end{aligned} \quad (\text{C.1})$$

where $Y_{L/R}$ are the hypercharges of the left/right-handed fields interacting with the hypercharge gauge boson B_μ , $Q_B = 1/3$ is the charge of the quarks under the baryon force, $\mu_{B'} = 3g_B v_B$ is the mass term generated after the spontaneous breaking of $U(1)_B$ and $\sin\epsilon$ parametrizes the kinetic mixing between both Abelian gauge bosons B_μ and B'_μ .

There are different paths to bring the kinetic terms in the first line of Eq. (C.1) to an orthonormal form via a non-orthogonal transformation. For convenience, we choose a change of basis that does not modify the well-known relation between the neutral SM gauge bosons, this can be achieved through the following transformation of the B_μ and B'_μ fields:

$$\begin{pmatrix} B_\mu \\ B'_\mu \end{pmatrix} \mapsto \begin{pmatrix} 1 & -\tan\epsilon \\ 0 & \sec\epsilon \end{pmatrix} \begin{pmatrix} B_\mu \\ B'_\mu \end{pmatrix} \quad (\text{C.2})$$

which renders the kinetic Lagrangian for the gauge bosons orthonormalized and leads to the following mass terms

$$\begin{aligned} \mathcal{L} \supset & \frac{1}{8}v_0^2 (g_2W_{3\mu} - g_1(B_\mu - \tan\epsilon B'_\mu)) (g_2W_{3\mu} - g_1(B^\mu - \tan\epsilon B'^\mu)) \\ & + \frac{1}{2}\mu_{B'}^2 \sec^2\epsilon B'_\mu B'^\mu, \end{aligned} \quad (\text{C.3})$$

with the mass matrix in the neutral gauge boson basis (W_μ^3, B_μ, B'_μ)

$$M_0^2 = \frac{1}{4} \begin{pmatrix} g_2^2 v_0^2 & -g_1 g_2 v_0^2 & g_1 g_2 \tan\epsilon v_0^2 \\ -g_1 g_2 v_0^2 & g_1^2 v_0^2 & -g_1^2 \tan\epsilon v_0^2 \\ g_1 g_2 \tan\epsilon v_0^2 & -g_1^2 \tan\epsilon v_0^2 & g_1^2 \tan^2\epsilon v_0^2 + 4\mu_{B'}^2 \sec^2\epsilon \end{pmatrix}. \quad (\text{C.4})$$

Now, by rotating the W_3^μ and B^μ fields as it is done in the SM,

$$\begin{pmatrix} B_\mu \\ W_{3\mu} \end{pmatrix} = \begin{pmatrix} \cos\theta_W^0 & -\sin\theta_W^0 \\ \sin\theta_W^0 & \cos\theta_W^0 \end{pmatrix} \begin{pmatrix} A_\mu \\ C_\mu \end{pmatrix}, \quad (\text{C.5})$$

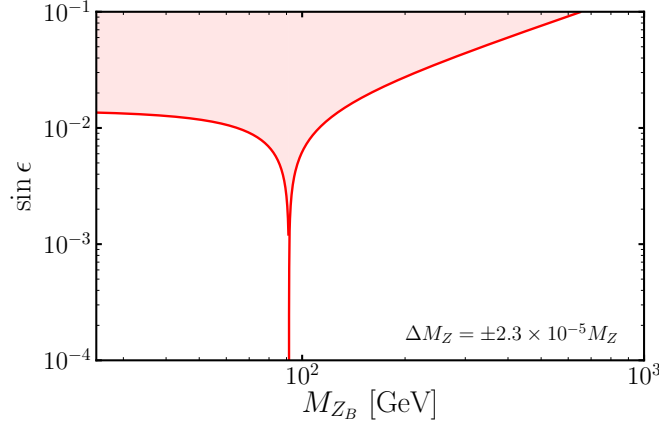


Figure 14: Experimental constraint on the kinetic mixing, $\sin \epsilon$, as a function of the Z_B mass. We have used the measurement of the Z boson mass.

where

$$\cos \theta_W^0 \equiv \frac{g_2}{\sqrt{g_1^2 + g_2^2}}, \quad \text{and} \quad \sin \theta_W^0 \equiv \frac{g_1}{\sqrt{g_1^2 + g_2^2}},$$

the photon decouples and we are left with the following mass matrix for the still unphysical neutral gauge bosons C_μ and B'_μ :

$$M_0^2 = \frac{1}{4} \begin{pmatrix} 0 & 0 & 0 \\ 0 & (g_1^2 + g_2^2)v_0^2 & \sqrt{g_1^2 + g_2^2} g_1 \tan \epsilon v_0^2 \\ 0 & \sqrt{g_1^2 + g_2^2} g_1 \tan \epsilon v_0^2 & 4\mu_{B'}^2 \sec^2 \epsilon + g_1^2 \tan^2 \epsilon v_0^2 \end{pmatrix}. \quad (\text{C.6})$$

The above mass matrix defines the angle of the final rotation towards the physical basis,

$$\begin{aligned} C_\mu &= \cos \xi Z_\mu + \sin \xi Z_{B\mu} \\ B'_\mu &= -\sin \xi Z_\mu + \cos \xi Z_{B\mu} \end{aligned} \quad (\text{C.7})$$

given by

$$\tan 2\xi = \frac{2g_1 \sqrt{g_1^2 + g_2^2} \tan \epsilon v_0^2}{4\mu_{B'}^2 \sec^2 \epsilon + g_1^2 \tan^2 \epsilon v_0^2 - (g_1^2 + g_2^2)v_0^2}, \quad (\text{C.8})$$

with the following eigenvalues defining their masses:

$$M_{A_\mu}^2 = 0, \quad (\text{C.9})$$

$$\begin{aligned} M_{Z,Z_B}^2 &= \frac{1}{8} (g_1^2 \sec^2 \epsilon + g_2^2) v_0^2 + \frac{1}{2} \mu_{B'}^2 \sec^2 \epsilon \\ &\pm \frac{1}{8} \sqrt{(4\mu_{B'}^2 \sec^2 \epsilon + (g_1^2 \sec^2 \epsilon + g_2^2)v_0^2)^2 - 16(g_1^2 + g_2^2)\mu_{B'}^2 v_0^2 \sec^2 \epsilon}, \end{aligned} \quad (\text{C.10})$$

as expected, in the limit $\epsilon \rightarrow 0$ we recover the original masses in the Lagrangian for Z and Z_B .

We can now apply the high precision measurement of the Z boson mass to constrain the kinetic mixing parameter, $\sin \epsilon$. The 1σ uncertainty in the experimentally measured Z boson mass is [3]

$$\frac{\Delta M_Z}{M_Z^{\text{SM}}} = \frac{M_Z - M_Z^{\text{SM}}}{M_Z^{\text{SM}}} \leq \pm 2.3 \times 10^{-5}, \quad (\text{C.11})$$

and this can be used to constrain the shift induced by the kinetic mixing. In Fig. 14 we show this constraint in the M_{Z_B} vs $\sin \epsilon$ plane; as can be seen, the kinetic mixing has to be very small and it does not change the main results in our paper. Recently, the CMS [38] and the LHCb [39] collaborations found stronger constraints for this mixing parameter for $M_{Z_B} \leq 200$ GeV by searching for the direct production of a new gauge boson.

References

- [1] ATLAS collaboration, G. Aad et al., *Observation of a new particle in the search for the Standard Model Higgs boson with the ATLAS detector at the LHC*, *Phys. Lett. B* **716** (2012) 1–29, [[1207.7214](#)].
- [2] CMS collaboration, S. Chatrchyan et al., *Observation of a New Boson at a Mass of 125 GeV with the CMS Experiment at the LHC*, *Phys. Lett. B* **716** (2012) 30–61, [[1207.7235](#)].
- [3] PARTICLE DATA GROUP collaboration, M. Tanabashi et al., *Review of Particle Physics*, *Phys. Rev. D* **98** (2018) 030001.
- [4] M. Cepeda et al., *Report from Working Group 2*, *CERN Yellow Rep. Monogr.* **7** (2019) 221–584, [[1902.00134](#)].
- [5] A. Pais, *Remark on baryon conservation*, *Phys. Rev. D* **8** (1973) 1844–1846.
- [6] R. Foot, G. C. Joshi and H. Lew, *Gauged Baryon and Lepton Numbers*, *Phys. Rev. D* **40** (1989) 2487–2489.
- [7] C. D. Carone and H. Murayama, *Realistic models with a light $U(1)$ gauge boson coupled to baryon number*, *Phys. Rev. D* **52** (1995) 484–493, [[hep-ph/9501220](#)].
- [8] P. Fileviez Perez and M. B. Wise, *Baryon and lepton number as local gauge symmetries*, *Phys. Rev. D* **82** (2010) 011901, [[1002.1754](#)].
- [9] P. Fileviez Perez and M. B. Wise, *Breaking Local Baryon and Lepton Number at the TeV Scale*, *JHEP* **08** (2011) 068, [[1106.0343](#)].
- [10] M. Duerr, P. Fileviez Perez and M. B. Wise, *Gauge Theory for Baryon and Lepton Numbers with Leptoquarks*, *Phys. Rev. Lett.* **110** (2013) 231801, [[1304.0576](#)].
- [11] P. Fileviez Perez, S. Ohmer and H. H. Patel, *Minimal Theory for Lepto-Baryons*, *Phys. Lett. B* **735** (2014) 283–287, [[1403.8029](#)].
- [12] P. Fileviez Perez, *New Paradigm for Baryon and Lepton Number Violation*, *Phys. Rept.* **597** (2015) 1–30, [[1501.01886](#)].
- [13] M. Duerr and P. Fileviez Perez, *Theory for Baryon Number and Dark Matter at the LHC*, *Phys. Rev. D* **91** (2015) 095001, [[1409.8165](#)].

- [14] S. Ohmer and H. H. Patel, *Leptobaryons as Majorana Dark Matter*, *Phys. Rev. D* **92** (2015) 055020, [[1506.00954](#)].
- [15] M. Duerr, P. Fileviez Perez and J. Smirnov, *Baryonic Higgs at the LHC*, *JHEP* **09** (2017) 093, [[1704.03811](#)].
- [16] P. Fileviez Perez, E. Golias, R.-H. Li and C. Murgui, *Leptophobic Dark Matter and the Baryon Number Violation Scale*, *Phys. Rev.* **D99** (2019) 035009, [[1810.06646](#)].
- [17] P. Fileviez Perez, E. Golias, R.-H. Li, C. Murgui and A. D. Plascencia, *Anomaly-free dark matter models*, *Phys. Rev.* **D100** (2019) 015017, [[1904.01017](#)].
- [18] M. Carena, M. Quirós and Y. Zhang, *Dark CP Violation and Gauged Lepton/Baryon Number for Electroweak Baryogenesis*, *Phys. Rev.* **D101** (2020) 055014, [[1908.04818](#)].
- [19] CMS collaboration, A. M. Sirunyan et al., *Search for Low-Mass Quark-Antiquark Resonances Produced in Association with a Photon at $\sqrt{s}=13$ TeV*, *Phys. Rev. Lett.* **123** (2019) 231803, [[1905.10331](#)].
- [20] CMS collaboration, V. Khachatryan et al., *Search for narrow resonances in dijet final states at $\sqrt{s}=8$ TeV with the novel CMS technique of data scouting*, *Phys. Rev. Lett.* **117** (2016) 031802, [[1604.08907](#)].
- [21] CMS collaboration, A. M. Sirunyan et al., *Search for narrow resonances in the b-tagged dijet mass spectrum in proton-proton collisions at $\sqrt{s}=8$ TeV*, *Phys. Rev. Lett.* **120** (2018) 201801, [[1802.06149](#)].
- [22] CMS collaboration, A. M. Sirunyan et al., *Search for low mass vector resonances decaying into quark-antiquark pairs in proton-proton collisions at $\sqrt{s}=13$ TeV*, *Phys. Rev.* **D100** (2019) 112007, [[1909.04114](#)].
- [23] CMS collaboration, A. M. Sirunyan et al., *Search for narrow and broad dijet resonances in proton-proton collisions at $\sqrt{s}=13$ TeV and constraints on dark matter mediators and other new particles*, *JHEP* **08** (2018) 130, [[1806.00843](#)].
- [24] CMS collaboration, A. M. Sirunyan et al., *Search for dijet resonances using events with three jets in proton-proton collisions at $\sqrt{s}=13$ TeV*, [1911.03761](#).
- [25] ATLAS collaboration, M. Aaboud et al., *Search for low-mass dijet resonances using trigger-level jets with the ATLAS detector in pp collisions at $\sqrt{s}=13$ TeV*, *Phys. Rev. Lett.* **121** (2018) 081801, [[1804.03496](#)].
- [26] A. Alloul, N. D. Christensen, C. Degrande, C. Duhr and B. Fuks, *FeynRules 2.0 - A complete toolbox for tree-level phenomenology*, *Comput. Phys. Commun.* **185** (2014) 2250–2300, [[1310.1921](#)].
- [27] J. Alwall, R. Frederix, S. Frixione, V. Hirschi, F. Maltoni, O. Mattelaer et al., *The automated computation of tree-level and next-to-leading order differential cross sections, and their matching to parton shower simulations*, *JHEP* **07** (2014) 079, [[1405.0301](#)].
- [28] A. D. Martin, W. J. Stirling, R. S. Thorne and G. Watt, *Parton distributions for the LHC*, *Eur. Phys. J.* **C63** (2009) 189–285, [[0901.0002](#)].
- [29] A. Ilnicka, T. Robens and T. Stefaniak, *Constraining Extended Scalar Sectors at the LHC and beyond*, *Mod. Phys. Lett.* **A33** (2018) 1830007, [[1803.03594](#)].
- [30] ATLAS, CMS collaboration, G. Aad et al., *Measurements of the Higgs boson production*

and decay rates and constraints on its couplings from a combined ATLAS and CMS analysis of the LHC pp collision data at $\sqrt{s} = 7$ and 8 TeV, *JHEP* **08** (2016) 045, [[1606.02266](#)].

- [31] LHC HIGGS CROSS SECTION WORKING GROUP collaboration, D. de Florian et al., *Handbook of LHC Higgs Cross Sections: 4. Deciphering the Nature of the Higgs Sector*, [1610.07922](#).
- [32] G. Apollinari, I. Béjar Alonso, O. Brüning, P. Fessia, M. Lamont, L. Rossi et al., *High-Luminosity Large Hadron Collider (HL-LHC)*, *CERN Yellow Rep. Monogr.* **4** (2017) 1–516.
- [33] ATLAS collaboration, M. Aaboud et al., *Observation of $H \rightarrow b\bar{b}$ decays and VH production with the ATLAS detector*, *Phys. Lett. B* **786** (2018) 59–86, [[1808.08238](#)].
- [34] CMS collaboration, A. M. Sirunyan et al., *Evidence for the Higgs boson decay to a bottom quark–antiquark pair*, *Phys. Lett. B* **780** (2018) 501–532, [[1709.07497](#)].
- [35] J. M. Butterworth, A. R. Davison, M. Rubin and G. P. Salam, *Jet substructure as a new Higgs search channel at the LHC*, *AIP Conf. Proc.* **1078** (2009) 189–191, [[0809.2530](#)].
- [36] K. S. Babu, C. F. Kolda and J. March-Russell, *Implications of generalized Z - Z-prime mixing*, *Phys. Rev. D* **57** (1998) 6788–6792, [[hep-ph/9710441](#)].
- [37] A. Hook, E. Izaguirre and J. G. Wacker, *Model Independent Bounds on Kinetic Mixing*, *Adv. High Energy Phys.* **2011** (2011) 859762, [[1006.0973](#)].
- [38] CMS collaboration, CMS Collaboration, *Search for a narrow resonance decaying to a pair of muons in proton-proton collisions at 13 TeV*, .
- [39] LHCb collaboration, R. Aaij et al., *Search for Dark Photons Produced in 13 TeV pp Collisions*, *Phys. Rev. Lett.* **120** (2018) 061801, [[1710.02867](#)].